First-Principles Calculation of Third-Order Elastic Constants via Numerical Differentiation of the Second Piola-Kirchhoff Stress Tensor

Tengfei Cao, David Cuffari, and Angelo Bongiorno

Phys. Rev. Lett. **121**, 216001 — Published 21 November 2018

DOI: 10.1103/PhysRevLett.121.216001

First-principles calculation of third-order elastic constants via numerical differentiation of the second Piola-Kirchhoff stress tensor

Tengfei Cao,[1,2] David Cuffari,[1,3] and Angelo Bongiorno*[1,2,3,4]

[1] *Department of Chemistry, College of Staten Island, Staten Island, NY 10314*
[2] *Advanced Science Research Center, City University of New York, 85 St Nicholas Terrace, New York, New York 10031*
[3] *Ph.D. Program in Physics, The Graduate Center of the City University of New York, New York, NY 10016*
[4] *Ph.D. Program in Chemistry, The Graduate Center of the City University of New York, New York, NY 10016*

A general method is presented to calculate from *first principles* the full set of third-order elastic constants of a material of arbitrary symmetry. The method here illustrated relies on a plane-wave density functional theory scheme to calculate the Cauchy stress, and numerical differentiation of the second Piola-Kirchhoff stress tensor to evaluate the elastic constants. It is shown that finite difference formulas lead to a cancellation of the finite basis set errors, whereas simple solutions are proposed to eliminate numerical errors arising from the use of Fourier interpolation techniques. Applications to diamond, silicon, aluminum, magnesium, graphene, and a graphane conformer give results in excellent agreement with both experiments and previous calculations based on fitting energy density curves, demonstrating both accuracy and generality of our new methodology to investigate nonlinear elastic behaviors of materials.

PACS numbers:

Third-order elastic constants (TOECs) are important physical parameters characterizing the nonlinear elastic behavior of a material [1]. Knowledge of TOECs allows one to estimate long-wavelength phonon anharmonicities [2], the generalized Grüneisen parameters [3], and the intrinsic mechanical strength of a material [1, 4]. In this work, we present a general and accurate method to calculate from *first principles* the full set of TOECs of a material of arbitrary symmetry.

TOECs of bulk materials are typically obtained from ultrasonic velocity measurements [5]. These experiments are difficult and produce data with large error margins, sometimes up to 50% or more [6]. In addition, TOECs are far more structure sensitive than the second-order elastic constants (SOECs), and sample quality is known to introduce variability in the experimental data [2, 7–10]. As a result, so far TOECs have been measured for only a relatively few bulk materials [2, 7–10]. In recent years, nanoindentation experiments have also been used to probe linear and nonlinear elastic properties of 2D materials [11, 12]. Unfortunately, these measurements allow to extract effective (or averaged) elastic moduli (for a 2D material treated as a homogeneous and isotropic membrane), whose relationships with the individual SOECs and TOECs of the crystalline film are unclear [13] and remain a topic of extensive research [12]. This experimental situation demands for computational methods to calculate and predict TOECs, particularly of materials for which experiments cannot be easily or accurately performed.

Methods are available to calculate TOECs from first principles [9, 13–18]. These methods rely on the use of supercells and finite homogeneous deformations, an energy scheme to calculate either energy-strain or stress-strain curves, symmetry relationships to express the energy or stress versus strain curves in terms of combinations of SOECs and TOECs, and a fitting procedure to extract the values of the independent SOECs and TOECs of the crystalline material. Dating back to the work of Naimon *et al.* [14], these methods have been applied mostly to cubic [9, 17, 18] or hexagonal crystals [13, 15, 16]. More recently, this type of method was also applied to a triclinic crystal [9], reaching a satisfactory agreement with the experimental data. Overall, this body of work has led to identify two major pitfalls of these methods. First, fitting energy-density (or stress) versus strain curves with polynomials is an onerous operation, leading to results that may vary depending on both the width of the interval of strain values and the convergence of the density functional theory (DFT) calculations. Second and most important, these methods are applicable only to highly symmetric crystals, for which the energy-strain or stress-strain curves can be conveniently expressed in terms of a selected number of independent elastic constants. Here, we introduce a novel method based on first principles calculations that is both accurate and applicable to a broad class of systems, including 3D or 2D low-symmetry crystals, as well as defected and inhomogeneous materials.

The present method relies on periodic DFT calculations and the application of finite homogeneous deformations to a supercell. In this context, we can define the

deformation gradient F_{ij} as:

$$F_{ij} = \frac{\partial x_i}{\partial X_j} = V'_{ik} V^{-1}_{kj}, \quad (1)$$

with the first equality providing the general definition of F_{ij} in terms of spatial (x_i) and material (X_j) coordinates, and where $\mathbf{V}'$ and $\mathbf{V}$ are 3×3 matrices whose columns are the vectors $\vec{a}'_1, \vec{a}'_2, \vec{a}'_3$ and $\vec{a}_1, \vec{a}_2, \vec{a}_3$, defining the geometries of the supercells and real space lattices of the deformed and reference materials systems, respectively. Within the framework of finite (or large) strain theory, the symmetric Lagrangian elastic strain ε_{ij} is defined as [1]:

$$\varepsilon_{ij} = \frac{1}{2}(F_{ki}F_{kj} - \delta_{ij}), \quad (2)$$

with δ_{ij} the Kronecker's delta, whereas the internal energy U at fixed entropy to third order in strain is written as follows:

$$\begin{aligned} U &= \frac{1}{2!}\frac{\partial^2 U}{\partial\varepsilon_{ij}\partial\varepsilon_{lm}}\varepsilon_{ij}\varepsilon_{lm} + \frac{1}{3!}\frac{\partial^3 U}{\partial\varepsilon_{ij}\partial\varepsilon_{lm}\partial\varepsilon_{pq}}\varepsilon_{ij}\varepsilon_{lm}\varepsilon_{pq} \\ &= \frac{1}{2}C^{(2)}_{ijlm}\varepsilon_{ij}\varepsilon_{lm} + \frac{1}{6}C^{(3)}_{ijlmpq}\varepsilon_{ij}\varepsilon_{lm}\varepsilon_{pq}, \end{aligned} \quad (3)$$

where $C^{(2)}_{ijlm}$ and $C^{(3)}_{ijlmpq}$ are the SOECs and TOECs of the material at the unstressed reference state. Cauchy stress σ_{ij} and second Piola-Kirchhoff (2^{nd}-PK) stress P_{lm} are related to each other via the following equation:

$$\sigma_{ij} = \frac{V}{V'}F_{il}P_{lm}F_{jm}, \quad (4)$$

where V' and V are the volumes of the deformed and reference supercells, respectively, and the 2^{nd}-PK stress tensor is written in terms of elastic constants and Lagrangian strain as [1]:

$$P_{ij} = C^{(2)}_{ijlm}\varepsilon_{lm} + \frac{1}{2}C^{(3)}_{ijlmpq}\varepsilon_{lm}\varepsilon_{pq}. \quad (5)$$

The equations above constitute the basis of our method to calculate TOECs by using periodic DFT calculations. In particular, we select the value of the Lagrangian strain tensor, and we use Eqs. 2 and 1 to derive F_{ij} and V'_{ik}. Then, we use a periodic DFT scheme to calculate the Cauchy stress tensor of the supercell accommodating the deformation. Equation 4 is then used to derive the 2^{nd}-PK stress tensor, and numerical differentiation of Eq. 5 is carried out to calculate the values of both the SOECs and TOECs. In particular, using Voigt's notation ($C^{(2)}_{ijlm} \leftrightarrow C^{(2)}_{\alpha\beta}$ and $C^{(3)}_{ijlmpq} \leftrightarrow C^{(3)}_{\alpha\beta\gamma}$, where the Greek indices run from 1 to 6, with $xx \rightarrow 1, yy \rightarrow 2, zz \rightarrow 3, yz \rightarrow 4, xz \rightarrow 5, xy \rightarrow 6$), the finite difference formula to calculate a SOEC is:

$$C^{(2)}_{\alpha\beta} = \frac{\partial P_\alpha}{\partial\varepsilon_\beta} = \frac{P_\alpha^{(+\Delta\varepsilon_\beta)} - P_\alpha^{(-\Delta\varepsilon_\beta)}}{2\Delta\varepsilon_\beta}, \quad (6)$$

where $P_\alpha^{(\pm\Delta\varepsilon_\beta)}$ is the component α of the 2^{nd}-PK tensor of the supercell accommodating the finite strain $\pm\Delta\varepsilon_\beta$. To calculate TOECs, we have two cases. First, when at least two out of three indices are equal, we can use:

$$C^{(3)}_{\alpha\beta\beta} = \frac{\partial^2 P_\alpha}{\partial^2\varepsilon_\beta} = \frac{P_\alpha^{(+\Delta\varepsilon_\beta)} + P_\alpha^{(-\Delta\varepsilon_\beta)} - 2P_\alpha^{(0)}}{{\Delta\varepsilon_\beta}^2}, \quad (7)$$

where $P_\alpha^{(0)}$ refers to the component of the 2^{nd}-PK stress tensor of the unstressed reference material. Second, when $\beta \neq \gamma$, we use

$$\begin{aligned} C^{(3)}_{\alpha\beta\gamma} &= \Big(P_\alpha^{(+\Delta\varepsilon_\beta,+\Delta\varepsilon_\gamma)} - P_\alpha^{(-\Delta\varepsilon_\beta,+\Delta\varepsilon_\gamma)} - \\ &\quad P_\alpha^{(+\Delta\varepsilon_\beta,-\Delta\varepsilon_\gamma)} + P_\alpha^{(-\Delta\varepsilon_\beta,-\Delta\varepsilon_\gamma)}\Big)/4\Delta\varepsilon_\beta\Delta\varepsilon_\gamma, \end{aligned} \quad (8)$$

where the elements of the 2^{nd}-PK tensor are computed for a deformed supercell accommodating two types of finite deformations, $\pm\Delta\varepsilon_\beta$ and $\pm\Delta\varepsilon_\gamma$. Equation 6 has been used to calculate SOECs from first principles [15, 16]. Here, we show that second-order numerical differentiation of the 2^{nd}-PK stress tensor allows to design an efficient, accurate, and general method to calculate the full set of TOECs of a material from first principles calculations. In this method, each elastic constant is calculated independently, by using either Eq. 7 or Eq. 8, by carrying out a minimal number of calculations. Symmetry relations can be exploited to reduce the number of calculations or, as in the present work, to verify the correctness of the method implementation. In the following, we validate and apply an implementation of our method based on the use of a conventional pseudopotential plane-wave DFT approach [19]. All DFT calculations here presented are carried out using primitive unit cells, dense uniform meshes of k points to sample the Brillouin zones, norm-conserving pseudopotentials [20], and a generalized gradient approximation for the exchange and correlation energy functional [21]. In all calculations, atomic positions are relaxed and fully optimized using a convergence threshold on the total force of 10^{-6} a.u. At the end of each calculation, ions occupy fixed positions, and the temperature is 0 K. Further technical details of the calculations are provided in the figure and table captions.

To demonstrate the validity and accuracy of our method, we consider the case of diamond, whose TOECs have been repeatedly measured and calculated over the past years [9, 10, 16]. Figure 1 shows the energy density and component $P_1 \leftrightarrow P_{xx}$ of the 2^{nd}-PK stress tensor of a diamond crystal at 0 K under uniaxial strain in the x direction. These energy and pressure data allow to calculate $C^{(2)}_{11}$ and $C^{(3)}_{111}$ [9, 10, 16]. A fitting of the energy curve gives values of 1037 GPa and -5876 GPa, respectively. Identical results are derived from Eqs. 6 and 7 by using the values of P_1 for the unstressed crystal and those obtained with a percent uniaxial strain of either

$\pm 0.5\%$ or $\pm 1\%$ (Fig. 1). These results show that finite differentiation of the 2^{nd}-PK tensor is a viable technique to calculate both SOECs and TOECs.

Periodic DFT schemes are based on expanding the wavefunctions in terms of a truncated basis set, most commonly a plane wave basis set [19, 22]. In plane-wave based DFT methods, the stress tensor is calculated as derivative of the energy at fixed number of plane waves [15, 22], and not at fixed energy cutoff [23–25]. Consequently, when using moderate plane-wave energy cutoffs, the diagonal elements of the Cauchy stress tensor are underestimated by the so-called Pulay corrective terms [23–25]:

$$\sigma_{ij}^{p} = -\frac{2}{3}\frac{\partial E}{\partial \ln E_c}\delta_{ij}, \tag{9}$$

where E_c is the plane-wave energy cutoff and E is the energy per unit volume.

Figure 2 shows the value of $C_{144}^{(3)}$ of diamond obtained by using Eq. 7 and employing stress tensors obtained from DFT calculations of unstressed and shear strained supercells at increasing energy cutoffs E_c. In particular, we use finite shear strains of $\Delta\varepsilon_4 = \pm 0.005$, and we calculate the selected TOEC by using 2^{nd}-PK stress tensors that are calculated by either accounting or not for the Pulay corrective terms in Eq. 9. The results in Fig. 2 show that the value of $C_{144}^{(3)}$ is subjected to large errors, regardless of the Pulay corrections, thereby showing that these errors do not arise from the use of a finite basis set or the stress formalism implemented in our DFT scheme. Figure 2 and additional calculations show also that these errors do not decrease in a regular manner for increasing E_c, and that they tend to be larger for small-valued TOECs. Interestingly, such a variability of results has also been obtained by using methods based on fitting energy-density versus strain curves.

The errors in Fig. 2 resulting from using Eq. 7 to calculate a small-value TOEC are algorithmic in nature. DFT methods based on plane waves utilize both a truncated discrete Fourier space and uniform real-space grids to store the value of wavefunctions and the charge density, and calculate the terms of the total energy, forces, and stress [15, 19, 22]. Due to the use of real-space grids, small differences in the stress components arise when, in case of crystals with a complex basis, the positions of the atoms within the supercell shift across the mesh of real-space points (Fig. 3). These differences become noticeable when we compare the stress tensor of an unstressed and shear strained crystal such as diamond (Fig. 3) or silicon. In these cases, a shear deformation leads to a breaking of the crystal symmetries, causing atoms in the unit cell to relax, change relative positions, and form inequivalent bonds [15, 26]. At a fixed energy cutoff, atoms within the unit cell of an unstressed crystal (typically) sits on top of points of the real-space grid, whereas such an alignment with grid points is lost in supercells accommodating a (shear) strain and a non-zero internal stress (Fig. 3). In brief, this shows that a plane-wave DFT calculation of an unstressed crystal differs, in numerical terms, from the calculations executed for the shear deformed states (Fig. 3). Differences in the numerical treatment translate into errors that can greatly affect the values of TOECs determined from stress-strain curves and numerical differention techniques (Fig. 2).

To eliminate the numerical errors resulting from the use of Eq. 7 and plane-wave based DFT methods, we propose two simple solutions. First, instead of using the components $P_{\alpha}^{(0)}$ computed by DFT for the unstressed state, in Eq. 7 we use values $\tilde{P}_{\alpha}^{(0)}$, obtained by extrapolation of values, $P_{\alpha}^{(\pm\Delta\varepsilon_\beta)}$, calculated for systems accommodating a small finite strain. As shown in both Figs. 2 and 3, this solution gives excellent results, yielding values of small-value TOECs that converge rapidly with the energy cutoff. Second, the numerical trick above is needed, or can be applied, to calculate the three TOECs with equal indices. In all other cases, any TOEC can be calculated by using Eq. 8, as for instance $C_{\alpha\beta\beta}^{(3)} = C_{\beta\alpha\beta}^{(3)}$. Equation 8 allows to estimate a TOEC with at least two unequal indices, without needing information about the unstressed state, and thus by using components of stress tensors computed under very similar "algorithmic" conditions. In the following applications of this method to calculate TOECs, we have adopted both solutions and verified that, within a few percent errors, they give the same results.

We use our method to calculate SOECs and TOECs at 0 K of three cubic crystals, namely diamond, silicon, and aluminum, and one hexagonal crystal, that is magnesium. The calculated SOECs and TOECs are reported in Table I together with experimental data measured at finite temperature. Our results shown in Table I compare well with both experimental data [3, 6–8, 10, 27] and previous DFT calculations [9, 10]. The agreement with the experiments is very good in the case of silicon and the metals, whereas it is satisfactory in case of diamond, for which the reported data show large variations and experimental uncertainties (Table I). In addition to applications to 3D crystals, we also use our method to calculate SOECs and TOECs at 0 K of two 2D crystals, namely graphene [13, 28] and washboard-graphane [28], a conformation of a fully hydrogenated graphene layer exhibiting a well-defined and regular arrangement of H atoms [28]. The latter 2D crystal has orthorhombic symmetry, with a rectangular unit cell containing 4 C-H bonds. Our method gives values of the SOECs and TOECs of these two 2D materials (Table II) that are in agreement with results of recent DFT calculations [28]. Experimental elastic constants are available only for graphene and a few other 2D membranes [11, 12]. The most accredited value for the 2D Young's modulus of

graphene is ∼340 N/m, although values between 20 and 700 N/m have been also reported [12]. Experimental estimates for the nonlinear elastic stiffness of graphene are also available [11, 12]. However, these elastic constants are extracted by fitting force versus indentation depth curves, and thus they cannot be directly compared to our calculated TOECs. Overall, our results in Table II show that our method can be used to predict SOECs and TOECs of complex materials such as graphane, for which the experimental determination of its elastic constants would be difficult to achieve. Furthermore, it is to be noted that our method gives the values of all the elastic constants, not only the independent ones. For instance, Table II reports the calculated value of -639 N m^{-1} for $C^{(3)}_{244}$, whereas using symmetry relations, its value should be $(2C^{(3)}_{111} - C^{(3)}_{222} - C^{(3)}_{112})/4$=-629 N m^{-1}. These checks allow to estimate a percent error on all elastic constants obtained with our method of about ±2%.

In conclusion, we have presented a method to calculate TOECs based on numerical differentiation of the second Piola-Kirchhof stress tensor. When used in conjunction with a periodic first principles approach, our method allows to predict the full set of TOECs, regardless of symmetry and structure of the periodic 3D or 2D material. Each elastic constant is calculated independently, by carrying out up to four first principles calculations. In this work, we have adopted a plane-wave DFT scheme to calculate stress values, and we have put forward simple solutions to overcome the errors resulting from the use of a truncated basis set and real-space grids. The applications to 3D and 2D crystals have demonstrated both the validity of our solutions and the overall accuracy of our method. This method and the ability to calculate the values of TOECs from first principles, not necessarily a plane-wave based DFT approach, will allow to predict nonlinear elastic behaviors of complex materials such as alloys, defected crystals, and 2D films [29], thereby impacting areas such as nanomechanics [29], nonlinear acoustics, and mechanical engineering.

We acknowledge the support of the NSF grant CMMI-1436375, the CUNY High Performance Computing Center, and the Extreme Science and Engineering Discovery Environment (XSEDE, NSF grant ACI-1548562) [30].

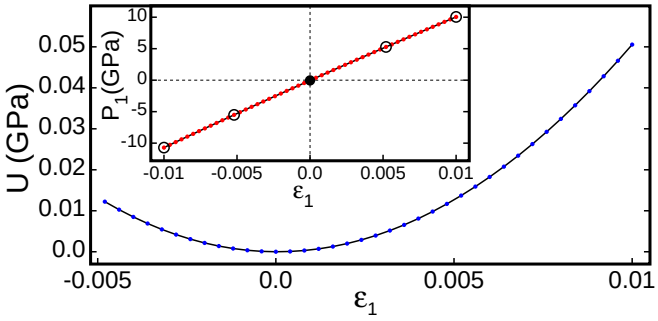

FIG. 1: Energy density U (Eq. 3) of diamond versus normal uniaxial (Lagrangian) strain ε_1. Inset, component P_1 of the 2^{nd}-PK stress tensor versus ε_1. Colored discs show the results obtained from DFT calculations [19] using an energy cutoff of 300 Ry. Solid lines are guides to the eye. To calculate $C^{(2)}_{11}$ and $C^{(3)}_{111}$, we use the value of P_1 at the unstressed state (large black disc) and those obtained at either $\varepsilon_1 = \pm 0.005$ or $\varepsilon_1 = \pm 0.010$ (circles).

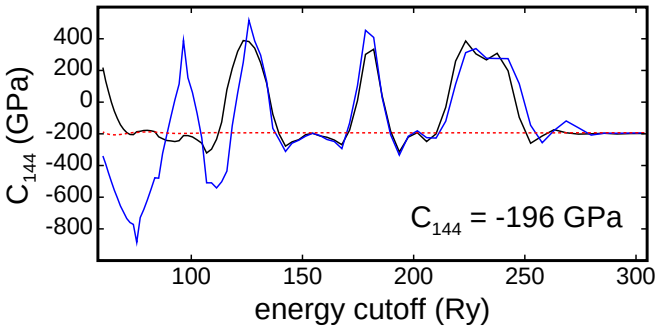

FIG. 2: $C^{(3)}_{144}$ of diamond obtained from Eq. 7 by using values of P_1 calculated by DFT at increasing energy cutoffs. $C^{(3)}_{144}$ is calculated by using the value of P_1 at an unstressed state, and values of P_1 of crystals accommodating a shear strain of $\varepsilon_4 = \pm 0.005$. The blue (black) colored solid line shows the results obtained by (not) including in the Cauchy stress the Pulay corrective terms of Eq. 9. Red colored dashed line shows the results obtained by replacing P_1 at the unstressed state in Eq. 7 with the value obtained by extrapolation from the values of P_1 at $\varepsilon_4 = \pm 0.005$ and ± 0.010.

TABLE I: Independent SOECs and TOECs (in GPa) of diamond, silicon, aluminum, and magnesium obtained by using Eqs. 6–8, and the numerical solutions described in the text. Experimental data are also shown for comparison. DFT calculations are carried out by using energy cutoffs of 100 Ry (diamond and silicon), 50 Ry (aluminum), and 30 Ry (magnesium). All calculations are carried out by using stringent convergence thresholds, and in case of the metals, we use fractional occupations and a smearing energy of 0.02 Ry.

	$C^{(2)}_{11}$	$C^{(2)}_{33}$	$C^{(2)}_{66}$	$C^{(2)}_{44}$	$C^{(2)}_{13}$	$C^{(2)}_{12}$	$C^{(3)}_{111}$	$C^{(3)}_{112}$	$C^{(3)}_{113}$	$C^{(3)}_{222}$	$C^{(3)}_{123}$	$C^{(3)}_{133}$	$C^{(3)}_{333}$	$C^{(3)}_{144}$	$C^{(3)}_{155}$	$C^{(3)}_{344}$	$C^{(3)}_{456}$
Diamond	1037	–	–	552	–	120	-5876	-1593	–	–	618	–	–	-197	-2739	–	-1111
Exp. Ref.[10]	1082	–	–	579	–	125	-7750	-2220	–	–	604	–	–	-1780	-2800	–	-30
Exp. Ref.[6]	–	–	–	–	–	–	-7603	-1909	–	–	835	–	–	1438	-3938	–	-2316
Silicon	142	–	–	72	–	51	-744	-393	–	–	-59	–	–	4	-297	–	-59
Exp. Ref.[27]	166	–	–	80	–	64	-795	-445	–	–	-75	–	–	15	-310	–	-86
Aluminum	108	–	–	33	–	59	-1100	-371	–	–	104	–	–	39	-421	–	-22
Exp. Ref.[7]	107	–	–	28	–	60	-1076	-315	–	–	36	–	–	-23	-340	–	-30
Magnesium	58	62	17	16	19	24	-602	-190	4	-762	-55	-107	-657	-60	-50	-163	–
Exp. Ref.[8]	59	62	17	16	–	26	-663	-178	30	-864	-76	-86	-726	-30	-58	-193	–

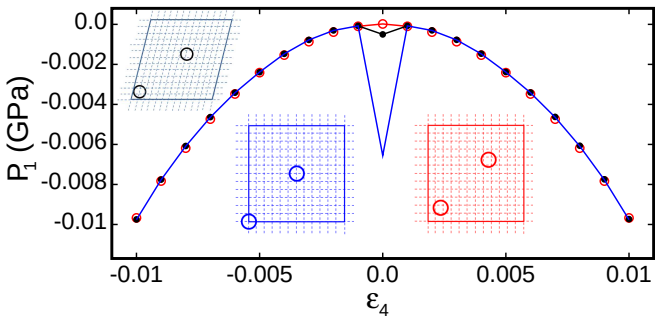

FIG. 3: Component P_1 of the 2^{nd}-PK stress tensor of a diamond crystal accommodating a shear strain ε_4. Discs show results obtained from DFT calculations carried out using energy cutoffs of 100 Ry (blue and black) and 200 Ry (red), with atoms in the unstressed primitive unit cell having fractional coordinates $(0,0,0)$ and $(0.25,0.25,0.25)$ (blue), and (x,y,z) and $(0.25+x,0.25+y,0.25+z)$ (black and red), where x,y,z are random numbers in the interval $(0,1)$. Insets, schematic representations of unstressed (blue and black) and shear strained (red) unit cells, with lattice coordinates that are (blue) or are not (black and red) aligned with the real-space grid of points used to represent wavefunctions in plane-wave based DFT calculations.

TABLE II: SOECs and TOECs (in N m^{-1}) of monolayer graphene (G) and washboard-graphane (W) calculated by using Eqs. 6–8. DFT calculations are carried out by using energy cutoffs of 100 Ry, and a vacuum region of 12 Å.

	$C^{(2)}_{11}$	$C^{(2)}_{22}$	$C^{(2)}_{12}$	$C^{(2)}_{44}$	$C^{(3)}_{111}$	$C^{(3)}_{222}$	$C^{(3)}_{112}$	$C^{(3)}_{122}$	$C^{(3)}_{144}$	$C^{(3)}_{244}$
G	348	348	59	144	-2920	-2873	-448	-515	-569	-639
W	276	162	21	80	-2580	-1211	-92	-295	-291	-405

[1] J. Clayton, *Nonlinear Mechanics of Crystals*, vol. 177 (Springer, Dordrecht, 2011).
[2] G. A. Saunders, H. B. Senin, H. A. A. Sidek, and J. Pelzl, Phys. Rev. B **48**, 15801 (1993).
[3] J. Philip and M. A. Breazeale, J. Appl. Phys. **54**, 752 (1983).
[4] J. Clayton, R. Kraft, and R. Leavy, Int. J. Solids Struct. **49**, 2686 (2012).
[5] R. Thurston and K. Brugger, Phys. Rev. **133**, 1604 (1964).
[6] J. M. Lang, Jr. and Y. M. Gupta, Phys. Rev. Lett. **106**, 125502 (2011).
[7] J. F. Thomas, Jr., Phys. Rev. **175**, 955 (1968).
[8] E. R. Naimon, Phys. Rev. B **4**, 4291 (1971).
[9] J. Zhao, J. M. Winey, and Y. M. Gupta, Phys. Rev. B **75**, 094105 (2007).
[10] A. V. Telichko, S. V. Erohin, G. M. Kvashnin, P. B. Sorokin, B. P. Sorokin, and V. D. Blank, J. Mater. Sci. **52**, 3447 (2017).
[11] C. Lee, X. Wei, J. Kysar, and J. Hone, Science **321**, 385 (2012).
[12] A. D, C. J. Brennan, J. S. Bunch, P. Egberts, J. R. Felts, H. Gao, R. Huang, J.-S. Kim, T. Li, Y. Li, et al., Extreme Mech. Lett. **13**, 42 (2017).
[13] E. Cadelano, P. L. Palla, S. Giordano, and L. Colombo, Phys. Rev. Lett. **102**, 235502 (2009).
[14] E. R. Naimon, T. Suzuki, and A. V. Granato, Phys. Rev. B **4**, 4297 (1971).
[15] O. H. Nielsen and R. M. Martin, Phys. Rev. B **32**, 3792 (1985).
[16] O. H. Nielsen, Phys. Rev. B **34**, 5808 (1986).
[17] A. Hmiel, J. M. Winey, Y. M. Gupta, and M. P. Desjarlais, Phys. Rev. B **93**, 174113 (2016).
[18] Y. K. Vekilov, O. M. Krasilnikov, A. V. Lugovskoy, and Y. E. Lozovik, Phys. Rev. B **94**, 104114 (2016).
[19] P. Giannozzi, S. Baroni, N. Bonini, M. Calandra, R. Car, C. Cavazzoni, D. Ceresoli, G. L. Chiarotti, M. Cococcioni, I. Dabo, et al., J. Phys.: Cond. Matter **21**, 395502 (2009).
[20] N. Troullier and J. L. Martins, Phys. Rev. B **43**, 1993 (1991).
[21] J. P. Perdew, K. Burke, and M. Ernzerhof, Phys. Rev. Lett. **77**, 3865 (1996).
[22] O. H. Nielsen and R. M. Martin, Phys. Rev. B **32**, 3780 (1985).
[23] P. Dacosta, H. Nielsen, and K. Kunc, J. Phys. C: Solid State Phys. **19**, 3163 (1986).
[24] S. Froyen and M. Cohen, J. Phys. C: Solid State Phys. **19**, 2623 (1986).
[25] G. Francis and M. Payne, J. Phys.: Cond. Matter **2**, 4395 (1990).
[26] E. B. Tadmor, G. S. Smith, N. Bernstein, and E. Kaxiras, Phys. Rev. B **59**, 235 (1999).
[27] J. J. Hall, Phys. Rev. **161**, 756 (1967).
[28] E. Cadelano, P. L. Palla, S. Giordano, and L. Colombo, Phys. Rev. B **82**, 235414 (2010).
[29] Y. Gao, T. Cao, F. Cellini, C. Berger, W. A. de Heer, E. Tosatti, E. Riedo, and A. Bongiorno, Nature Nanotech. **13**, 133 (2018).
[30] J. Towns, T. Cockerill, M. Dahan, I. Foster, K. Gaither, A. Grimshaw, V. Hazlewood, S. Lathrop, D. Lifka, G. D. Peterson, et al., Computing in Science & Engineering **16**, 62 (2014).